Journal of Membrane Science 573 (2019) 425–438

Contents lists available at ScienceDirect

Journal of Membrane Science

journal homepage: www.elsevier.com/locate/memsci

High-performance microporous polymer membranes prepared by interfacial polymerization for gas separation

Shuwen Yu[a,b,c], Shichun Li[b,d,*], Yu Liu[b], Sheng Cui[a,c,*], Xiaodong Shen[a,c]

[a] College of Materials Science and Engineering, Nanjing Tech University, Nanjing 210009, PR China
[b] Institute of Chemical Materials, China Academy of Engineering Physics, Mianyang 621900, PR China
[c] Jiangsu Collaborative Innovation Center for Advanced Inorganic Function Composites, Nanjing Tech University, Nanjing 210009, PR China
[d] Department of Materials Science and Metallurgy, University of Cambridge, Cambridge CB3 0FS, UK

ARTICLE INFO

Keywords:
Microporous polymer
Ultrathin membrane
Thin film composite (TFC)
Gas separation
Interfacial polymerization

ABSTRACT

Microporous polymers possessing good processability and low cost show promising applications for large-scale industrial membrane separation. The relatively low gas selectivity and physical aging of microporous polymer membranes are current challenges which become more serious for ultrathin membranes. Crosslinking is an effective way to improve gas selectivity and physical aging resistance of glassy polymers, and the cross-linked ultrathin membranes can be directly produced by interfacial polymerization (IP). However, there are only a few reports of IP formed microporous polymer membranes, and the reported gas separation performance is not satisfying. In this work, ultrathin microporous polyarylate (PAR) membranes were prepared by IP of 5,5′,6,6′-tetrahydroxy-3,3,3′,3′-tetramethylspirobisindane (TTSBI) and trimesoyl chloride (TMC). The crosslinking structure, molar ratio of TTSBI to TMC ($n_{(TTSBI)}/n_{(TMC)}$) in PAR, and membrane thickness characterized by zeta potential measurements, X-ray photoelectron spectroscopy and scanning electronic microscope were optimized by adjusting IP parameters such as pH value of aqueous phase that decides the hydrolysis of both TTSBI and TMC in IP, and the concentrations of TTSBI and TMC. The microporous structures of PAR characterized by CO_2 adsorption are highly relevant to the $n_{(TTSBI)}/n_{(TMC)}$ in PAR. The resulted membranes exhibit CO_2 permeance in a wide range of 100–2115 GPU with CO_2/N_2 selectivity of 45–21 that is a remarkable improvement in gas separation performance of IP formed microporous polymer membranes and also shows significant advantages over other reported ultrathin microporous polymer membranes. In addition, the membranes also exhibit excellent stability, and only 29% decrease in CO_2 permeance was observed after 180 h aging. This work provides an effective strategy to fabricate high-performance and stable microporous polymer membranes by IP, which is expected to push the particle applications of microporous polymer membranes in gas separation.

1. Introduction

The current chemical separation processes account for a large proportion, i.e. 10–15%, of the world's energy consumption [1]. Membrane-based separation that does not rely on heat would potentially use much less energy than traditional processes containing phase transition, e.g. distillation [1–4]. However, the membrane should exhibit better separation performance, i.e. higher permeance and selectivity, to achieve the goal of low energy consumption and low overall cost in several practical processes, for example, gas separation for energy gas supply and pollutant gas capture [2–4]. Considerable efforts have been made to fabricate membranes by using microporous materials, such as zeolites, carbon molecular sieve (CMS), metal organic frameworks (MOFs), covalent organic frameworks (COFs) and microporous polymers, as the permanent micro-pores in membrane could dramatically enhance the efficiency of molecule transport and separation, which provides considerably high permeance and selectivity of membranes [5,6]. Compared with the microporous inorganic materials and crystalline materials, microporous polymers show significant advantages of good processability and low cost which endow them with promising applications for large-scale industrial membrane separation [7,8].

Among microporous polymers, polymers of intrinsic microporosity (PIMs) and thermally rearranged (TR) polymers, due to unique combination of microporosity and solution processability, have been extensively investigated to fabricate membranes [6,7,9]. PIMs, initially investigated by McKeown, Budd and co-workers, contain highly rigid polybenzodioxane backbones and bulky side substituent that prevent

* Corresponding authors at: Institute of Chemical Materials, China Academy of Engineering Physics, Mianyang 621900, PR China.
E-mail addresses: lishichun@caep.cn (S. Li), scui@njtech.edu.cn (S. Cui).

https://doi.org/10.1016/j.memsci.2018.12.029
Received 13 July 2018; Received in revised form 23 November 2018; Accepted 9 December 2018
Available online 11 December 2018
0376-7388/

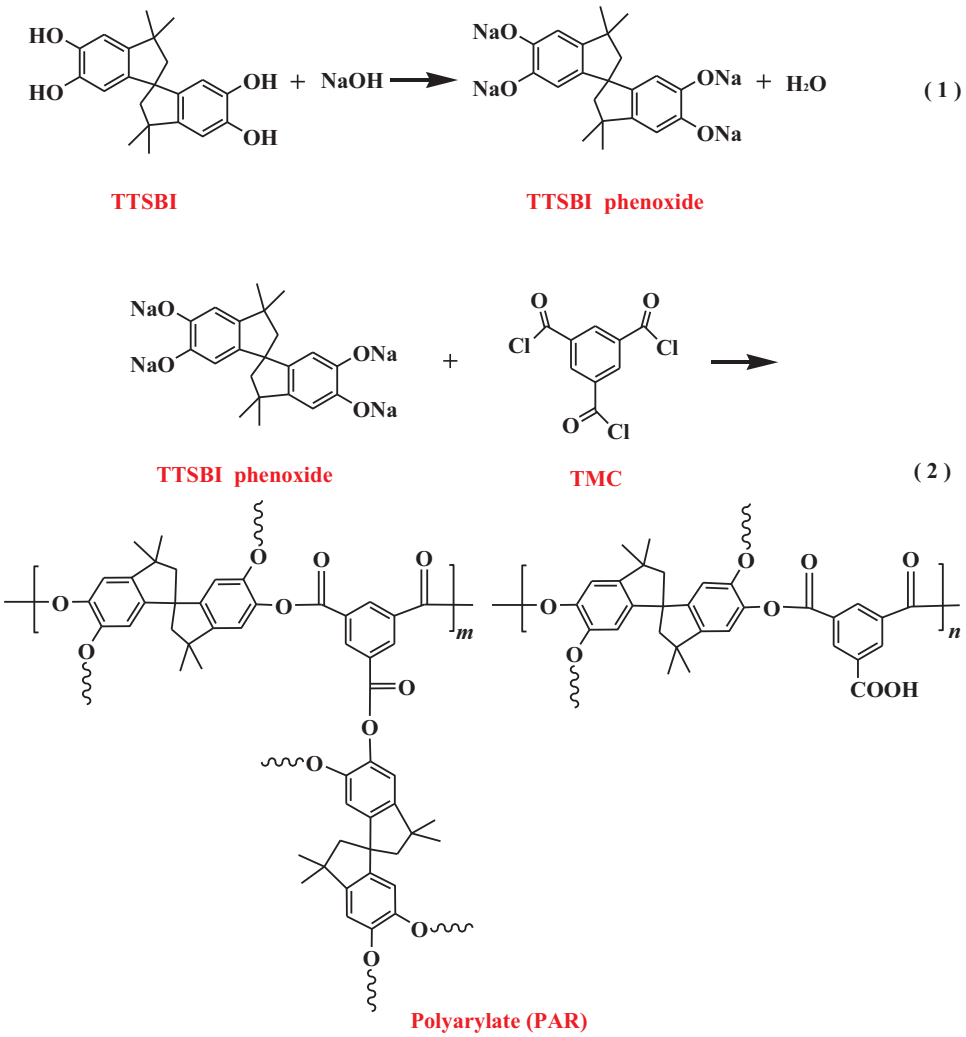

Scheme 1. The reaction of TTSBI and TMC to form spiro-structured PAR networks. (1) The formation of TTSBI phenoxide by the reaction of TTSBI and NaOH, and (2) the reaction of TTSBI phenoxide with TMC to form a spiro-structured PAR. Only the hydrolysis of TMC was presented here due to the complexity of the hydrolysis of TTSBI.

efficient chain packing and lead to an ultra-permeable polymer [10–14]. The CO_2 permeability of PIM membranes with thickness of 180 μm can reach 13,600 Barrers (1 Barrer = 1×10^{-10} cm^3 (STP) cm cm^{-2} s^{-1} $cmHg^{-1}$) with CO_2/N_2 selectivity of 18 [15]. As another representative microporous polymer, TR polybenzoxazole polymers, initially reported by Lee and co-workers, formed by the solid state thermal conversion of hydroxyl-containing polyimides to polybenzoxazoles [16]. The cavity sizes and size distributions of TR polymer membrane can be tailored through controlling the thermal reaction process and polymer chain structures, and the membrane could show remarkable CO_2 permeability and CO_2/N_2 selectivity [6,9,17–19].

The latest research has been focused on processing microporous polymers into defect-free ultrathin membranes with thickness lower than 1 μm that provides applicable gas flux [20–22]. The methods of coating and phase inversion are widely developed to fabricate ultrathin membranes with PIMs and TR polymers [23–29]. For example, Sivaniah et al. reported a 1-μm-thick mixed matrix membrane (MMM) based on PIM-1 and UiO-66-NH_2 particles, which was prepared by spin-coating on the surface of Anodisc flat disc membranes, and the CO_2 permeance reaches 1740 GPU (1 GPU = 1×10^{-6} cm^3 (STP) cm^{-2} s^{-1} cm Hg^{-1}) with CO_2/N_2 selectivity of 24 [25]. The phase inversion method named dry-jet/wet quench was well developed by Lee's group to make asymmetric TR polymer hollow fiber membranes [26,27,29,30]. The effective skin layer of TR polymer hollow fiber membrane is thinner than 1 μm, and the CO_2 permeance is around 2000 GPU with CO_2/N_2 selectivity of 13 [31].

Although the ultrathin microporous polymer membranes have exhibited very promising gas permeance, the selectivity still needs to be improved to fulfill the requirements of practical applications [32]. Moreover, the physical aging of the microporous polymer resulting in significantly losing gas permeability prevents the practical applications [33–37]. Unfortunately, the problems of low selectivity and physical aging become more serious for ultrathin membranes [25,38]. Crosslinking is an effective strategy to improve the gas selectivity and prevent the aging issue of glassy polymers, which has been applied for microporous polymer membranes [33,39–42]. However, neither coating nor phase inversion could directly process cross-linked polymers, since these methods require a good solubility of polymer in the solvent [20]. The post-modification of crosslinking complicates the membrane fabrication process.

Interfacial polymerization (IP), that has been extensively applied in production of large-scale industrial nanofiltration and reverse osmosis membranes [43,44], could directly produce cross-linked thin film composite (TFC) membranes, which is promising to fabricate ultrathin microporous polymer membranes with adequate crosslinking structures. Nevertheless, there are only a few reports of IP formed microporous polymer membranes. Moreover, the reported gas separation performance of IP formed microporous polymer membranes is not

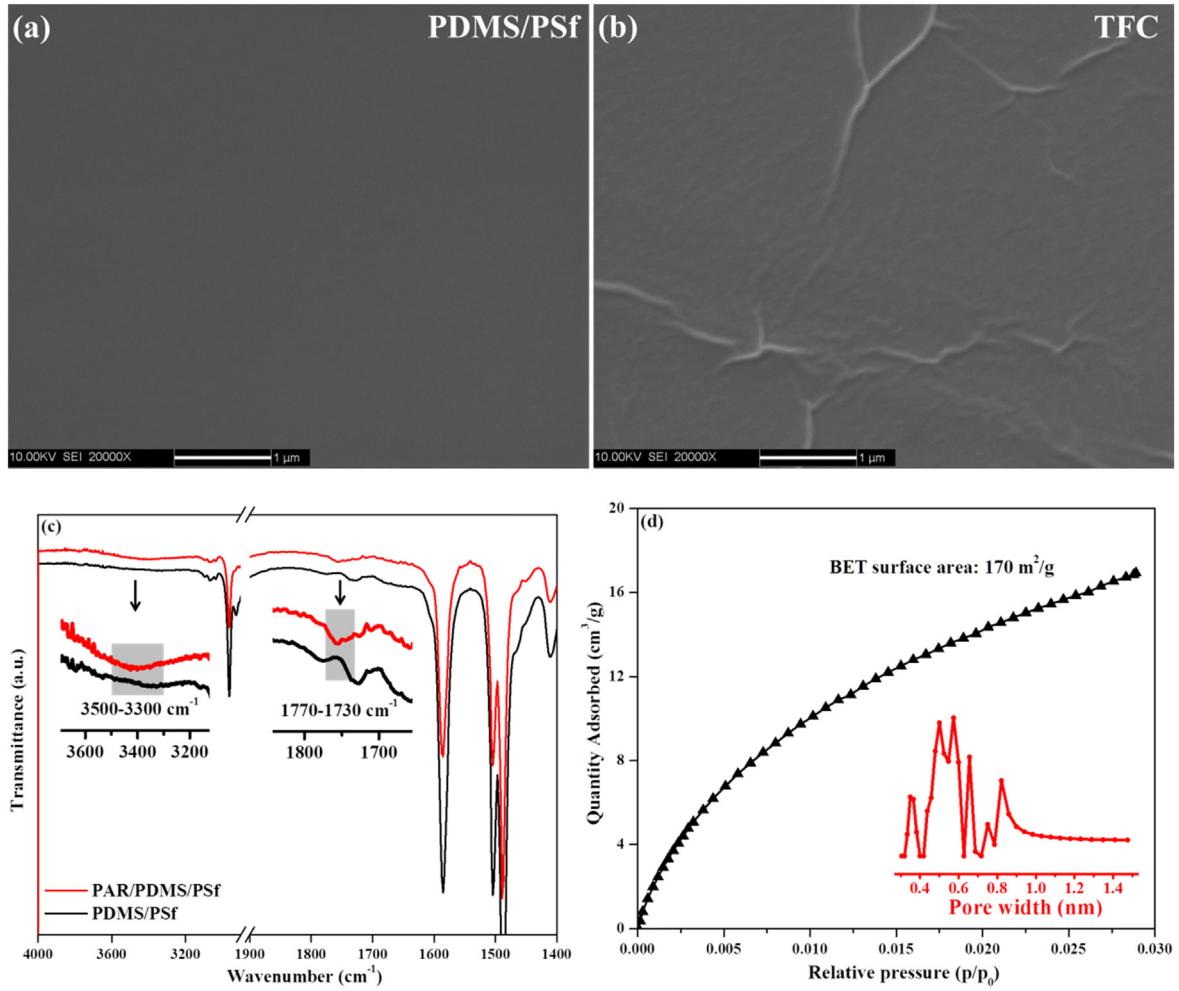

Fig. 1. (a-b) Surface SEM images and (c) ATR-FTIR spectra of PDMS/PSf membrane and microporous TFC membrane prepared with 0.25 mmol/L TMC in hexane, 10 mmol/L TTSBI and pH = 11.60 in aqueous phase; (d) CO_2 adsorption isotherm measured at 273 K for solid PAR-IP polymer powders prepared under pH = 11.60 in aqueous phase and the inset shows pore size distribution.

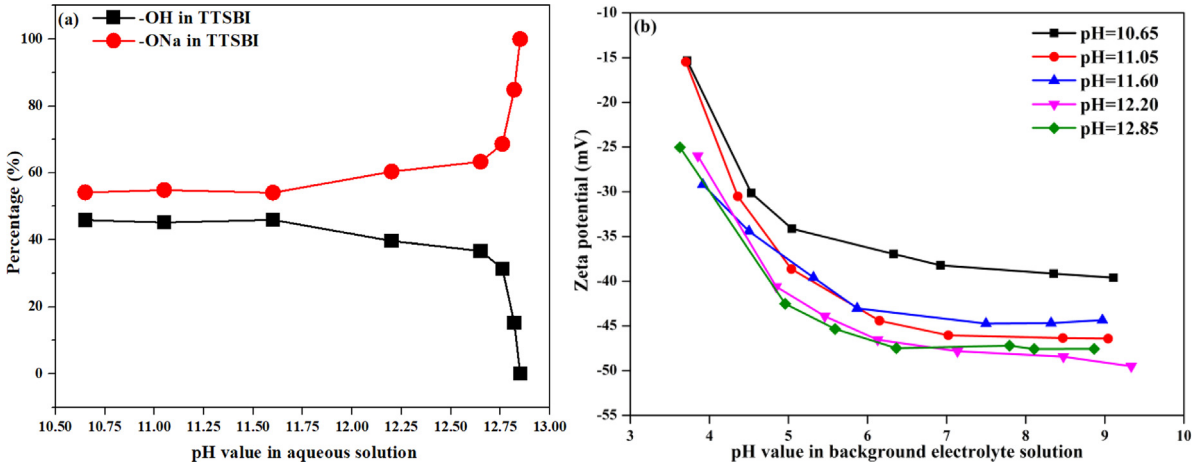

Fig. 2. (a) The content of –ONa and -OH groups of TTSBI in aqueous solution; (b) Surface zeta potentials of the microporous TFC membranes prepared with 0.25 mmol/L TMC in hexane and 10 mmol/L TTSBI in aqueous phase with different pH values.

satisfying [45,46]. Zhang et al. presented the preparation of microporous polyamides by IP for the first time, which showed excellent CO_2 capacity and CO_2/N_2 selectivity in gas adsorption test. But the acquired membranes contain defects and show no CO_2/N_2 selectivity [45]. Subsequently, Livingston et al. employed IP with contorted monomers, e.g. spiro-structured 5,5′,6,6′-tetrahydroxy-3,3,3′,3′-tetramethyl- spirobisindane (TTSBI) and cardo-structured 9,9-bis(4-hydroxyphenyl) fluorene (BHPF), to synthesize defect-free microporous polyarylate (PAR) nanofilms with thickness down to 20 nm on ultrafiltration supports [46]. The microporosity of PAR was well characterized by CO_2

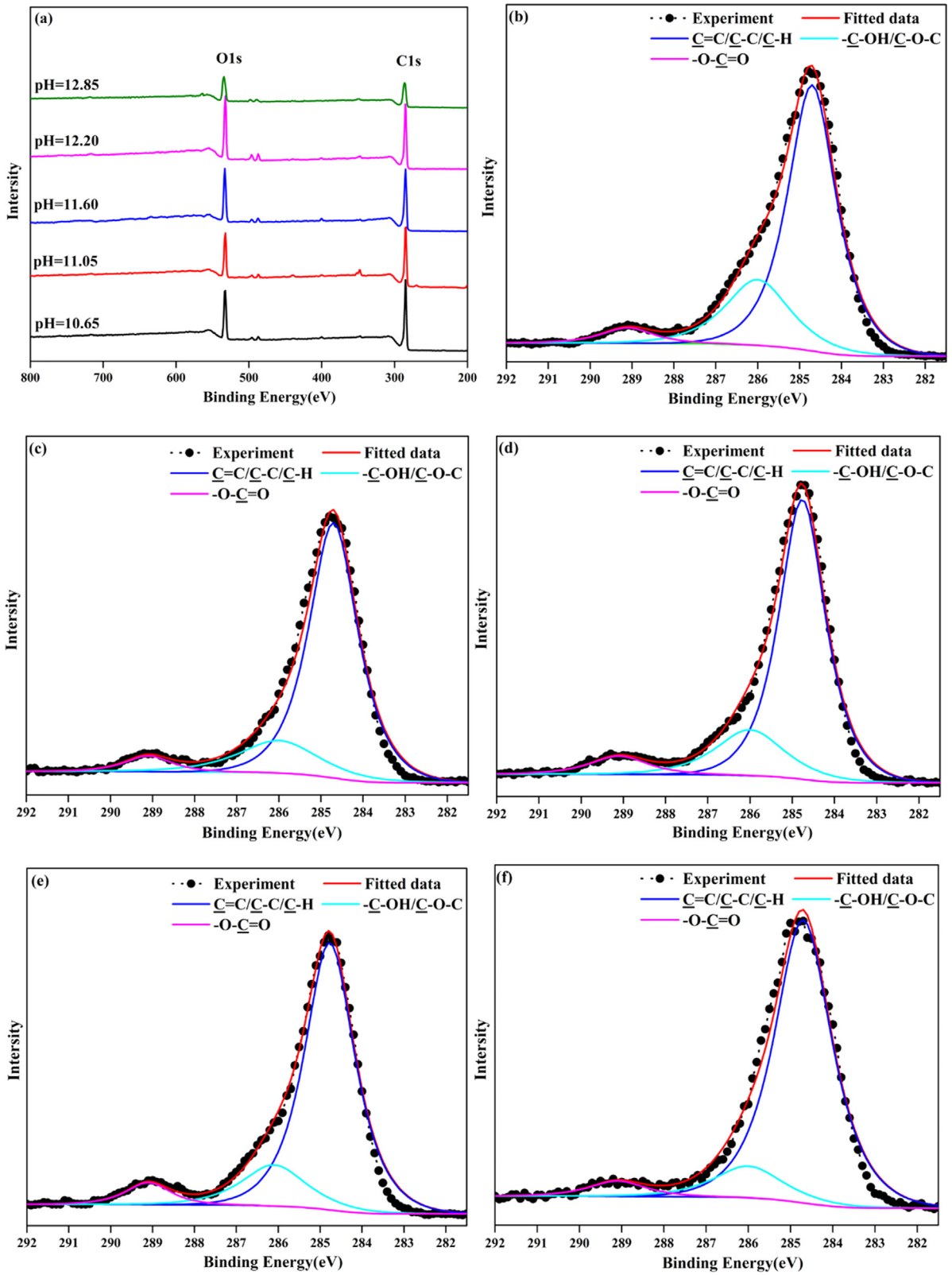

Fig. 3. (a) XPS spectra and (b-f) C1s narrow scan spectra of the microporous TFC membranes prepared with 0.25 mmol/L TMC in hexane and 10 mmol/L TTSBI in aqueous phase with pH = 10.65, 11.05, 11.60, 12.20 and 12.85, respectively.

adsorption, wide-angle X-ray scattering and molecular simulation. The surface area of PAR-TTSBI by monophasic reaction could reach 161.5 $m^2 g^{-1}$ measured from CO_2 adsorption, and the pores display the radius ranging from 1 to 7 Å and good interconnectivity. The resulted membranes possess excellent permeance of solvents in organic solvent nanofiltration (OSN) process, but the gas permeance is less than 100 GPU even for CO_2 and H_2 [46]. According to the formation-structure-performance correlation of IP formed gas separation membranes proposed by Wang et al., the gas permeance and selectivity could be enhanced via adjusting the preparation conditions in IP process which

Table 1
Percentages of the chemical species from the deconvolution of C1s narrow scan spectra of the microporous TFC membranes prepared with different pH values of aqueous solution.

	C=C/C-C/C-H (%)	C-OH/C-O-C (%)	O-C=O (%)	$n_{(TTSBI)}/n_{(TMC)}$ in PAR layer[a]
pH = 10.65	72.2	23.4	4.4	3.99
pH = 11.05	79.2	16.2	4.6	2.64
pH = 11.60	75.7	18.2	6.1	2.24
pH = 12.20	78.8	15.5	5.7	2.04
pH = 12.85	84.4	11.2	4.4	1.91

[a] The $n_{(TTSBI)}/n_{(TMC)}$ in PAR layer was calculated by the percentages of C-OH/C-O-C and O-C=O.

optimizes the membrane structures [47,48]. From this point, the IP formed microporous polymer membrane with high gas separation performance can be expected through IP condition optimization.

The aiming of this work is to fabricate high-performance ultra-thin microporous polymer membrane by IP. Spiro-structured PAR-TTSBI membrane was investigated in this work due to the appropriate microporous structure that suits gas molecule sieving [46]. The synthesis of PAR-TTSBI networks is illustrated in Scheme 1, in which only the hydrolysis of trimesoyl chloride (TMC) was considered due to the complexity of hydrolysis of TTSBI. The effects of pH value of aqueous phase in IP were investigated, as the pH value has a significant influence to the hydrolysis of both TTSBI and TMC during IP. Besides, the influence of monomer concentration was studied as well.

2. Materials and methods

2.1. Materials

Polysulfone (PSf) flat ultrafiltration membranes with an average surface pore radius of 17.9 nm and porosity of 4.85% (UFB30KF300, Pureach Technology, China) [49], polydimethylsiloxane (PDMS) (Shin-Etsu, Japan), tetraethoxysilane (TEOS, AR, Aladdin, China), ditinbutyldilautate (DBD, 95%, Aladdin, China), heptane (AR, Guanghua, China), hexane (AR, Guanghua, China), trimesoyl chloride (TMC, 99.5%, J&K, China), 5,5′,6,6′-tetrahydroxy-3,3,3′,3′-tetramethylspirobisindane (TTSBI, 97%, TCI, China), Tetrahydrofuran (THF, 99.11%, Superdry, Innochem, China), Pyridine (99.5%, Superdry, Innochem, China), $NaHCO_3$ and NaOH (AR, Aladdin, China).

2.2. Preparation of membranes and PAR polymer powders

The PDMS/PSf membranes were used as the substrates in IP. PDMS was used for plugging the pores on the surface of PSf and PDMS/PSf membranes were prepared according to our recent report [49]. The PDMS solution was prepared by dissolving 1 wt% PDMS, 1 wt% TEOS and 1 wt% DBD in heptane, followed by stirring for 40 min and standing for 30 min at 25 °C. The cross-linked PDMS solution was cast on PSf membranes with the size of 14 × 16 cm and the acquired PDMS/PSf membranes were kept in the artificial climate chamber at 30 °C with relative humidity of 40%. The CO_2 permeance and N_2 permeance of the PDMS/PSf membrane are 7780 GPU and 810 GPU, respectively [49].

The microporous TFC membranes were prepared by IP according to our previous reports [50]. During the IP process, the PDMS/PSf membrane was initially immersed into the organic solution for 3 min and then the excess solution was drained from the membrane surface. Afterwards, the impregnated membrane was placed into the aqueous solution for 3 min at 25 °C. After that, the membrane surface was washed with adequate deionized water and the resulting membranes were kept in the artificial climate chamber at 30 °C with relative humidity of 40%. The concentration of TMC in hexane was adjusted from 0.125 mmol/L to 1.25 mmol/L. The aqueous solution was prepared by adding TTSBI and additive, i.e. NaOH and $NaHCO_3$ into deionized water. The concentration of TTSBI was changed from 2 mmol/L to 30 mmol/L. The initial molar ratio of NaOH and TTSBI was 4:1 in aqueous solution, and then NaOH and/or $NaHCO_3$ were added to adjust pH value from 10.65 to 12.85. The detailed concentration of NaOH and $NaHCO_3$ are shown in Table S1.

The PAR polymer powders were synthesized by IP and monophasic polymerization [46], respectively, and the obtained polymers were named as PAR-IP and PAR-MP. PAR-IP was synthesized by IP of the TTSBI (10 mmol/L) in aqueous solution with pH = 10.65–12.20 and the TMC (0.25 mmol/L) in hexane under rigorous stirring for 3 min. The resulting polymers were then washed thoroughly with water by suction filtration. The polymers were dried at room temperature under vacuum for 48 h and then dried under vacuum for 12 h at 120 °C. In order to obtain PAR-MP, TTSBI was mixed with TMC dissolved in dry degassed THF. Afterwards, the dry pyridine was added through a syringe under nitrogen gas and stirring. After reflux for 20 h, the precipitate was washed with 1 M HCl solution, water and THF. It was subsequently dried through freeze drying, and then at 120 °C in a vacuum oven for 12 h. The detailed reaction conditions for monophasic polymerization reaction are listed in Table S2.

2.3. Structure characterization

Chemical structures of the membranes were characterized by attenuated total reflectance infrared (ATR-FTIR) spectroscopy (Nicolet 6700, Thermo Scientific) and X-ray photoelectron spectroscopy (XPS, ESCALAB 250). The X-Ray diffraction (XRD) measurement of PAR-IP and PAR-MP powders was collected with a Bruker D8 Advance diffractometer using Cu-K as radiation at 40 kV and 40 mA with a step of 0.02° per second. The zeta potentials of the membrane surface were tested using an Electro-kinetic Analyzer (Anton Paar GmbH, Austria). Morphologies of membranes were observed by scanning electronic microscope (SEM, CamScan Apollo 300). The thickness of membrane was analyzed on cross-sectional SEM images by ImageJ software. CO_2 sorption isotherms were performed at 273 K, in which the PAR-IP and PAR-MP were tested by Quantachrome Instruments and ASAP 2020, respectively. Samples were degassed at 120 °C under vacuum for 12 h before test.

2.4. Gas separation performance measurements

The gas permeance and selectivity were tested by a homemade apparatus described in the literature [47,50]. The membrane was mounted in a circular stainless steel cell and the effective membrane area is 19.26 cm^2. CO_2 pure gas, N_2 pure gas and CO_2/N_2 mixed gas (15% CO_2 and N_2 balance) were used as the feed gases. The mixed gas containing 15% CO_2 was chosen according to the content of CO_2 gas in flue gas [51,52]. In the test of wet gas, He was used as the sweep gas. The feed pressure varied from 0.2 MPa to 1.0 MPa. Prior to contacting the membranes, the feed gas was saturated with water vapor by bubbling through water bottle at 40 °C and then passing an empty bottle at 28 °C to remove the condensate water. The concentration of permeation gas was detected by gas chromatography (GC, Agilent 7890B) and the flow of outlet sweep gas was measured using a soap film meter (HY-5020–300 m). In the test of dry gases, the membrane was evacuated with a vacuum pump before measurements. Sweep gas was not used and the flow of outlet permeation gas was measured by using a soap film meter. The results were recorded as the mean values (± standard deviations) of three membrane samples prepared under the same condition.

3. Results and discussion

The surface morphologies of PDMS/PSf and microporous TFC membrane could be observed distinctly from SEM images in Fig. 1(a-b).

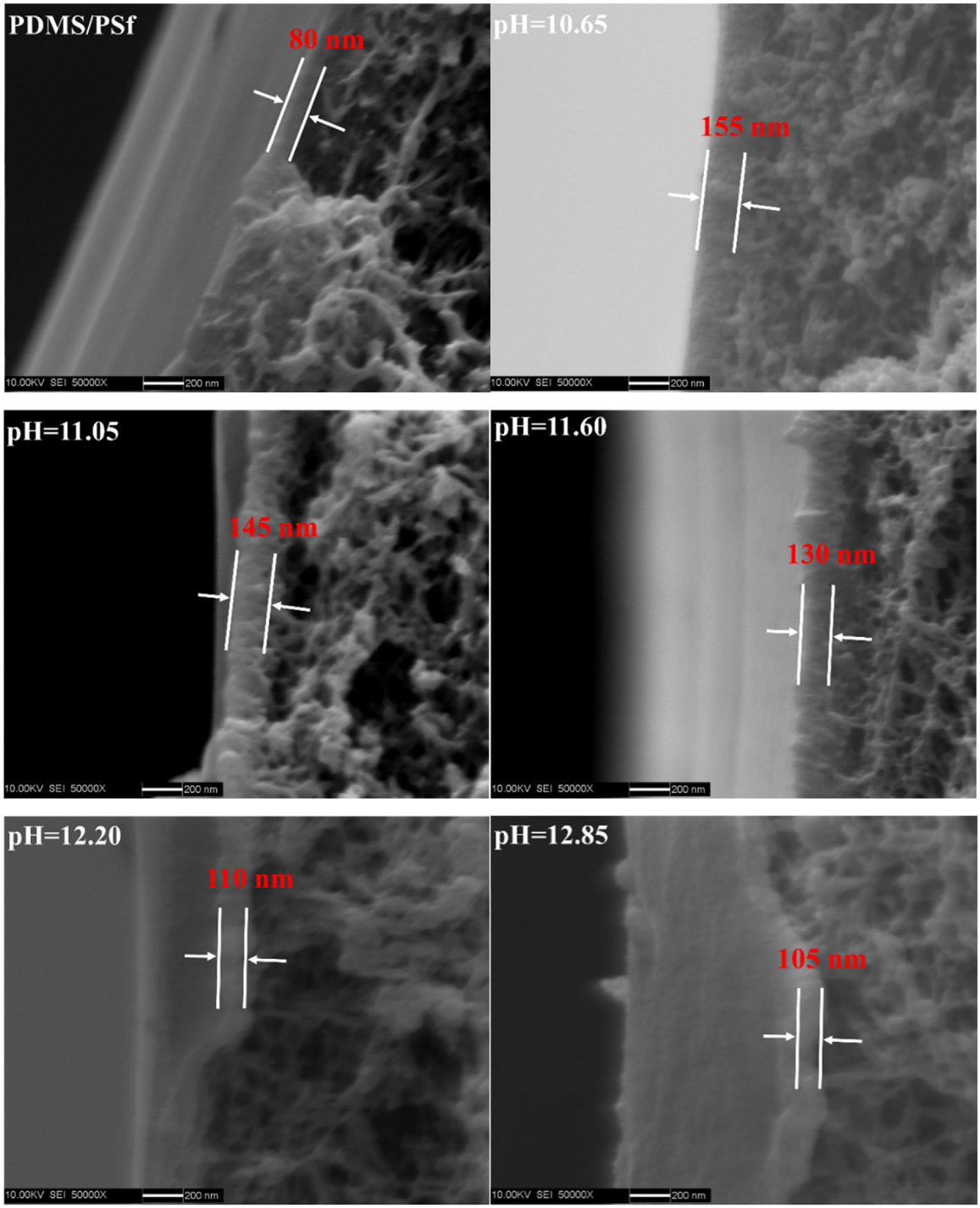

Fig. 4. Cross-sectional SEM images of PDMS/PSf membrane and microporous TFC membranes prepared with 0.25 mmol/L TMC in hexane and 10 mmol/L TTSBI in aqueous phase with different pH values.

The surface of PDMS/PSf membrane is smooth and compact without perceptible pores. After IP, there is a rough and crinkly active layer generated on the membrane surface, which is in accordance with literature [53]. Fig. 1(c) shows that the ATR-FTIR spectra of PDMS/PSf and TFC membrane. Compared with PDMS/PSf, the spectra of TFC membrane have additional peaks at 1770–1720 cm^{-1} corresponding to stretching of C=O in ester group formed by IP [47] and 3500–3300 cm^{-1} referring to unreacted hydroxyl groups (-OH) of TTSBI [54,55]. The CO_2 sorption isotherm of the PAR-IP polymer powders in Fig. 1(d) shows type I profile with characteristically steep uptake at low relative pressure [45], suggesting the microporous structure of the PAR networks with BET surface area of 170 m^2/g and pore size ranging from 5.0 to 8.2 Å. The lattice spacing of PAR-IP polymer powders by XRD corresponds with the level of microporosity observed in CO_2 sorption (Fig. S1 in Supporting information), which is also in accordance with literature [46]. The results indicated that a microporous PAR layer formed on PDMS/PSf after IP process.

3.1. Effects of pH value of aqueous phase

The pH value of aqueous phase in IP plays an important role on reaction process, membrane structure and gas permeation performance

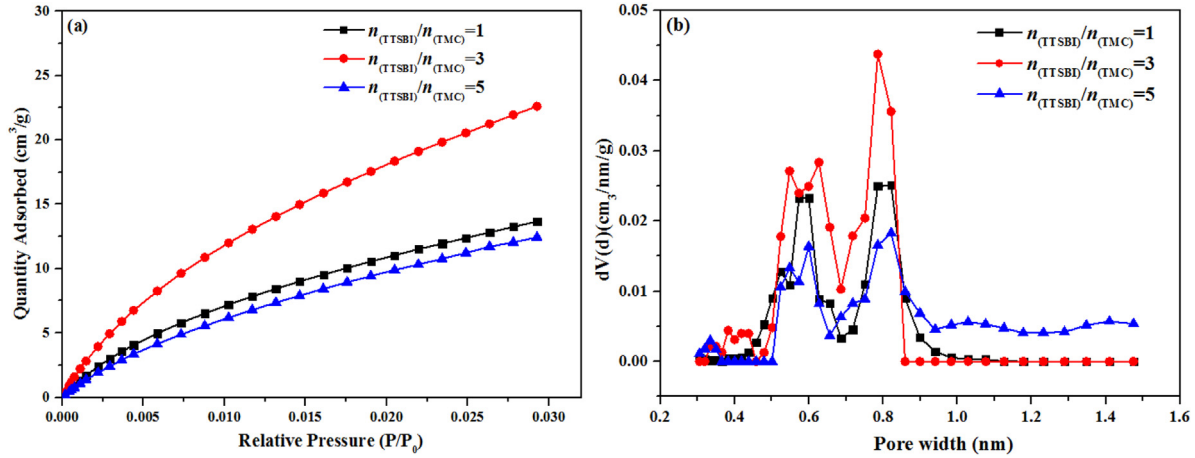

Fig. 5. (a) CO_2 adsorption isotherms measured at 273 K and (b) Pore size distribution calculated by DFT method for various solid PAR-MP polymers prepared with different $n_{(TTSBI)}/n_{(TMC)}$ in preparation solution.

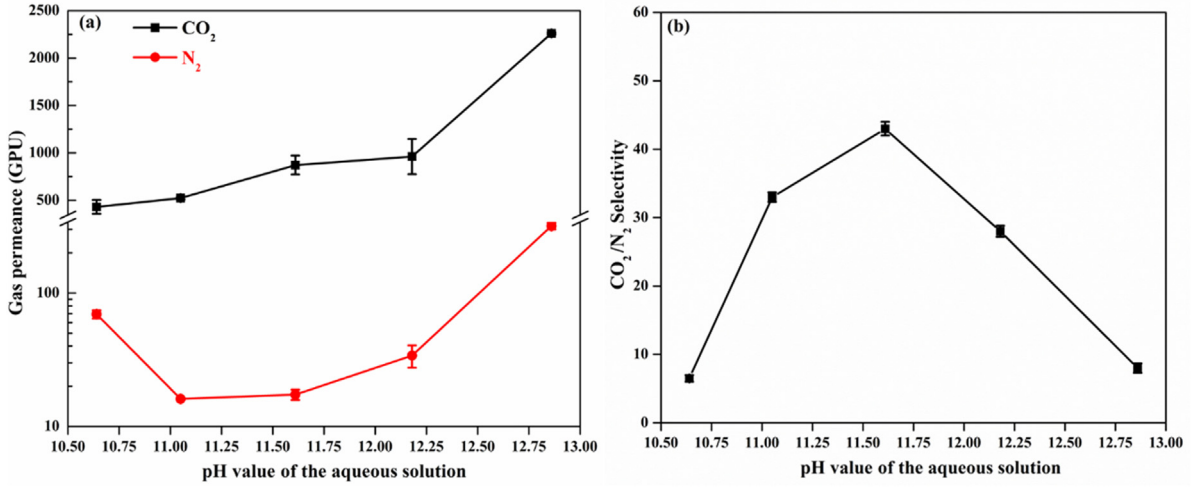

Fig. 6. Gas permeance (a) and CO_2/N_2 selectivity (b) of microporous TFC membranes prepared with 0.25 mmol/L TMC in hexane and 10 mmol/L TTSBI in aqueous phase with different pH values. Water saturated CO_2/N_2 mixed gas (15% CO_2 and N_2 balance) was used as the feed gas.

[56,57]. Generally, a relatively high pH value can neutralize the hydrochloric acid produced during the interfacial reaction that promotes toward a higher extent of crosslinking, but the strong alkaline environment will lead to the hydrolysis of TMC which is harmful for the crosslinking [56,57]. Although there is no hydrochloric acid produced during IP process in this work as shown in equation (2) in Scheme 1, the pH value can influence the dissolution and hydrolysis of TTSBI based on the equation (1) in Scheme 1. Thus, the number of reactive groups of TTSBI, i.e. -ONa, is possibly different under different pH value, which is obviously important to the IP process and membrane structure. Therefore, the pH value could remarkably affect the IP through hydrolysis of both TTSBI and TMC. A series of the microporous TFC membranes with 10 mmol/L TTSBI and 0.25 mmol/L TMC were prepared by changing pH value of aqueous solution from 10.65 to 12.85.

The percentages of -ONa groups and –OH groups in TTSBI under various pH value conditions were estimated according to the ionization constant of carbonate (See Table S1 in Supporting information), and the results are shown in Fig. 2(a). At pH value of 11.60, the content of –ONa group in TTSBI is 54%, and the content does not substantially change with decreasing pH value. This indicates that when the pH value is lower than 11.60, only about a half of functional groups of TTSBI could participate in the IP reaction, and the pH value hardly affects the content of reactive groups of TTSBI. When the pH value is higher than 11.60, the content of -ONa group in TTSBI rapidly increases with increasing pH value, and it reaches 100% at pH value of 12.85. The result indicates that more proportion of functional groups of TTSBI can participate in the IP reaction when the pH value is higher than 11.60, which is advantageous to increase the degree of crosslinking of the membrane.

In order to investigate the effects of pH value on hydrolysis of TMC, the zeta potential of the microporous TFC membranes was tested to verify the surface charge and the results are presented in Fig. 2(b). During the range of all tested pH values, all the zeta potential was negative, which is attributed to the –OH groups from the hydrolysis of TTSBI and –COOH groups from the hydrolysis of TMC. With increasing pH value of aqueous solution in IP, the zeta potential is more and more negative. The results indicate that the amount of negative charge groups on the surface of membrane increases with increasing pH value of aqueous solution. As shown in Fig. 2(a), however, the amount of –OH groups almost kept invariant with the pH value varying from 10.65 to 11.60, and then declines with increasing pH value of aqueous solution. Therefore, the decreasing zeta potential with increasing pH value of aqueous solution is mainly due to the increasing amount of -COOH groups, indicating increasing degree of TMC hydrolysis and unfavorable for the crosslinking of membrane.

XPS was used to analyze surface element composition of the microporous TFC membranes and the spectra are shown in Fig. 3. The two major peaks at 284.8 and 532.9 eV are ascribed to the binding energies

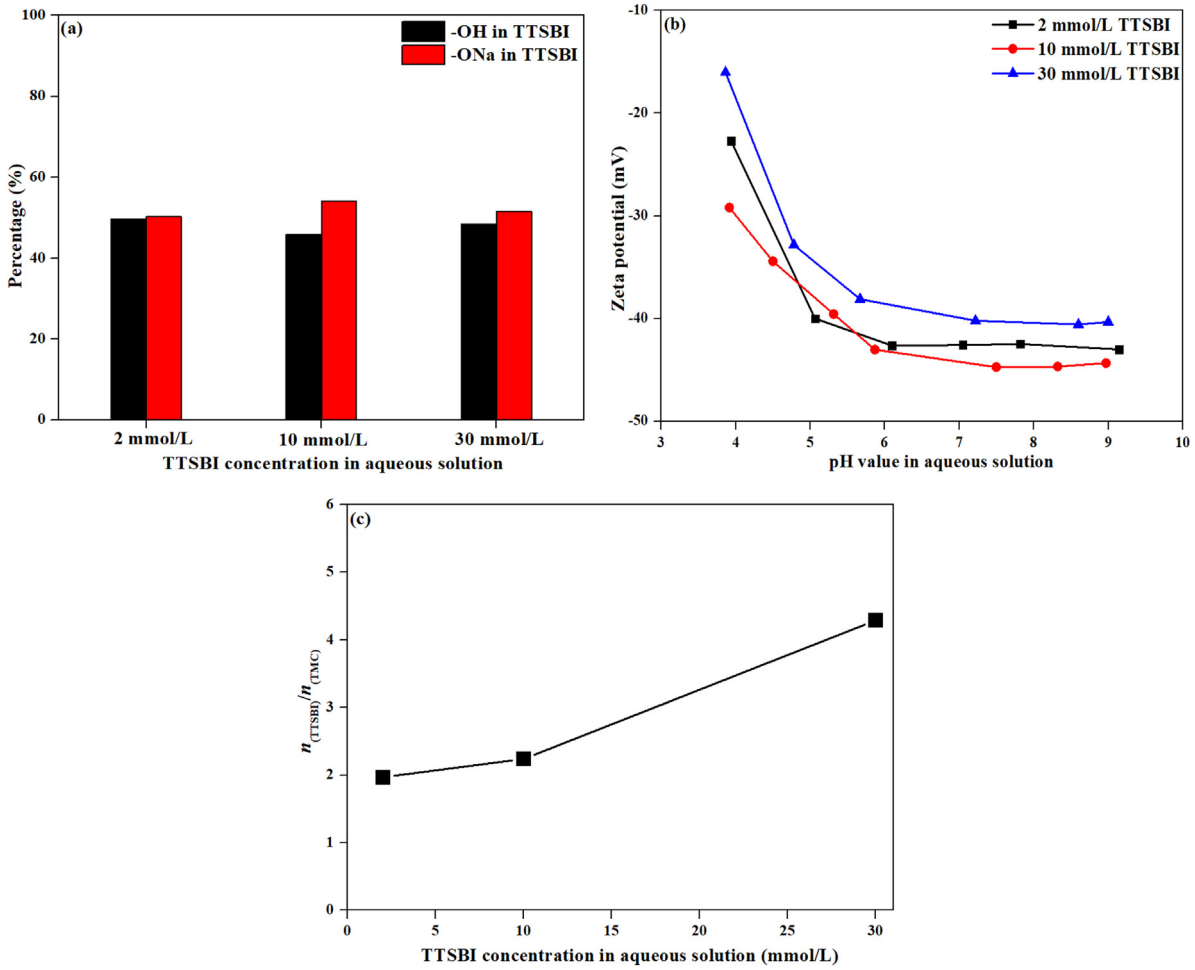

Fig. 7. (a) The content of –ONa and -OH in TTSBI, (b) Surface zeta potentials of the microporous TFC membranes and (c) The $n_{(TTSBI)}/n_{(TMC)}$ in PAR layer of membranes prepared with different TTSBI concentrations. All the pH value in aqueous phase is 11.60 and TMC concentration in hexane is 0.25 mmol/L.

of C1s and O1s, respectively. Deconvolution of C1s narrow scan spectrum was used to estimate the $n_{(TTSBI)}/n_{(TMC)}$ in PAR layers. The C1s narrow scan XPS spectra of the microporous TFC membranes prepared with different pH values and the corresponding percentages of the chemical species are shown in Fig. 3 and Table 1. As seen from Fig. 3, the C1s spectra of the membranes has three peaks at 284.7, 286.1 and 289.1, which represent the C=C/C- C/C-H, C-OH/C-O-C attributed to TTSBI and O-C=O attributed to TMC, respectively [58–60]. In Table 1, the $n_{(TTSBI)}/n_{(TMC)}$ in PAR layer decreases with increasing pH value of aqueous solution, which indicates that the content of TTSBI declines and TMC increases in PAR. The results are in accordance with the content of –ONa groups of TTSBI in aqueous solution and the surface zeta potentials of membranes. With increasing pH value, the amount of -ONa groups TTSBI increases leading to the declining amount of TTSBI in PAR, and the degree of TMC hydrolysis increases leading to the increase in TMC in PAR. It's worth to mention that the $n_{(TTSBI)}/n_{(TMC)}$ in PAR layer highly reaches 3.99 at pH value of 10.65, which is beyond the theoretical upper ratio, i.e. 3.00. It may be caused by the TTSBI particles contained in PAR. In order to decrease the pH value to 10.65, a large amount of $NaHCO_3$ was added to the aqueous solution (See Table S1 in Supporting information), which resulted in excessive ionic concentration of the solution and decrease in the solubility of TTSBI. A slight turbidity of the solution could be observed during the experiment due to the precipitation of TTSBI. The precipitated TTSBI may be packaged into PAR selective layer, resulting in a high $n_{(TTSBI)}/n_{(TMC)}$. In addition, the $n_{(TTSBI)}/n_{(TMC)}$ in Table 1 could not accurately reflect the actual proportion in PAR selective layer, and these data were used to analyze the trend of the changes in proportion.

The cross-sectional SEM images of the PDMS/PSf membrane and microporous TFC membranes are shown in Fig. 4. The thickness of PDMS/PSf membrane is about 80 nm and the result is in accordance with the report [49]. The PAR layer thickness in the microporous TFC membranes decreases from 75 nm to 25 nm with increasing pH value. The decrease in thickness was further verified by ATR-FTIR (see Fig. S2 in Supporting information). The reduced thickness of PAR layer could be caused by the hydrolysis of TMC which decreases the amount of TMC in IP [47].

According to the above results, the pH value in aqueous solution significantly affects the hydrolysis of both TTSBI and TMC, which results in the change of amounts of reactive groups of monomers in IP and then structures of formed PAR. With increasing pH value, the content of reactive groups in TTSBI, i.e. -ONa groups, remains unchanged first and then rises rapidly, but the content of reactive groups in TMC, i.e. acid chloride groups, decreases. The variation of the reactive groups of TTSBI and TMC leads to the decline of the $n_{(TTSBI)}/n_{(TMC)}$ in PAR layer, reflecting the fact that the crosslinking extent of the PAR changes with variation of the pH. In addition, the thickness of the PAR selective layer gradually decreases with increasing pH value. It can be estimated that the above variation of the PAR structure may also be accompanied with changes in the microporous structure of PAR [46]. As shown Fig. S3 in Supporting information, the CO_2 adsorption uptake of PAR-IP polymers prepared with different pH values fluctuates with increasing pH values, and the pore size distributions keep constant. The changes in CO_2 uptake of PAR-IP with increasing pH values could be attributed to both

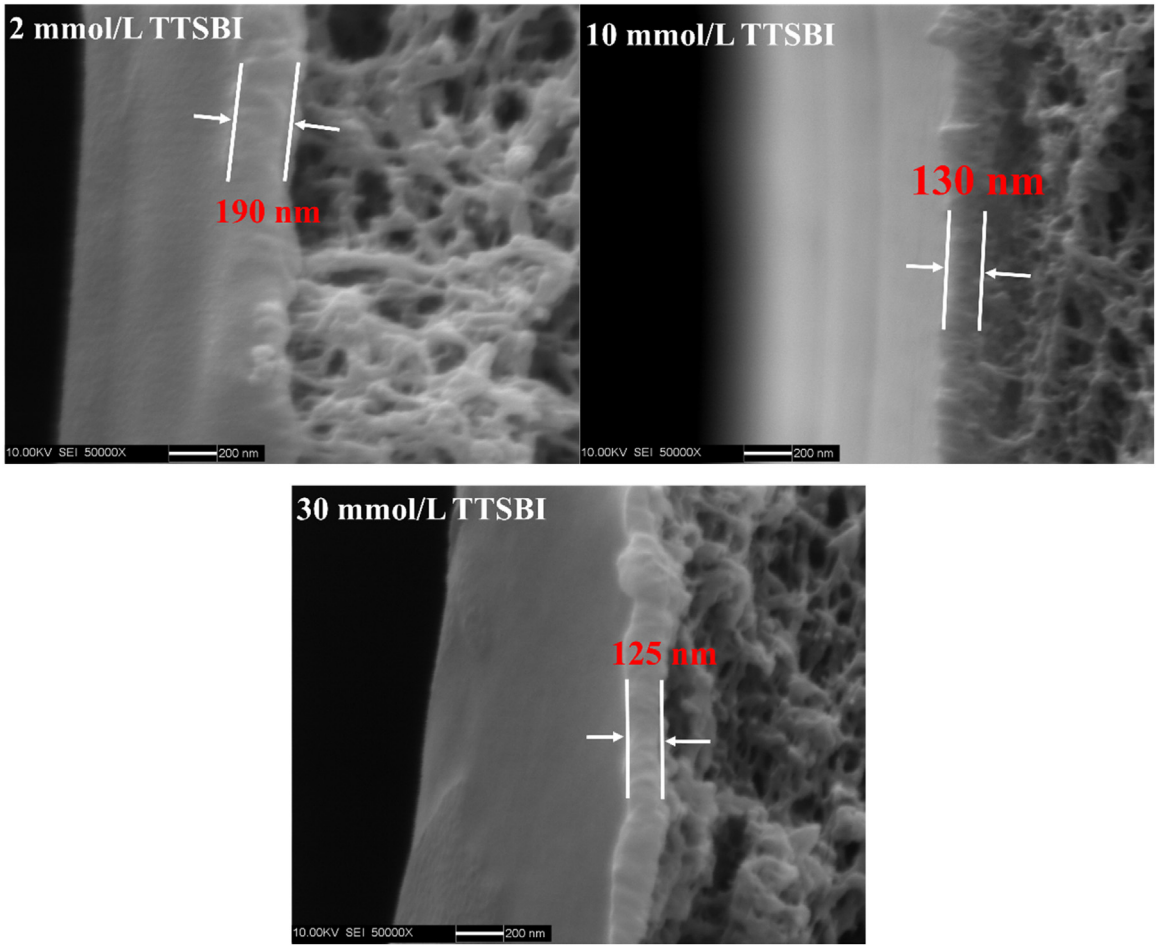

Fig. 8. Cross-sectional SEM images of microporous TFC membranes prepared with different TTSBI concentrations. All the pH value in aqueous phase is 11.60 and TMC concentration in hexane is 0.25 mmol/L.

changes in the microporous structures and the content of –OH groups and –COOH groups that formed from the hydrolysis of TTSBI and TMC and interact strongly with CO_2. In order to further confirm the changes in microporous structures of PAR with changing preparation conditions, the PAR-MP powders were prepared by monophasic polymerization reactions with different $n_{(TTSBI)}/n_{(TMC)}$. In the monophasic polymerization, the hydrolysis of monomers that happens in IP could be eliminated, which simplifies the factors affecting CO_2 uptake of PAR. The PAR-MP powders were characterized by FTIR, XPS, XRD and CO_2 adsorption shown in Fig. 5, Fig. S4 and Table S3. The results indicate that the microporous PAR-MP has been obtained as expected, and the $n_{(TTSBI)}/n_{(TMC)}$ in PAR-MP ranging from 1.12 to 2.93 is similar with that in PAR layer of TFC membrane. Fig. 5(a) show that the PAR-MP prepared with $n_{(TTSBI)}/n_{(TMC)}$ of 3 has the highest CO_2 uptake and the BET surface area reaches 222 cm^2/g. While, the pore size distributions of PAR-MP prepared with different $n_{(TTSBI)}/n_{(TMC)}$ are similar. The results indicate that the $n_{(TTSBI)}/n_{(TMC)}$ in PAR has a significant effect on the microporous structure of PAR, which could determine the gas separation performance of PAR membranes.

The effects of pH value on gas separation performance of membranes were investigated by using CO_2/N_2 mixed gas, and the results are presented in Fig. 6. With the increase of pH value, CO_2 permeance increases and N_2 permeance firstly decreases and then increases. The increasing CO_2 permeance is mainly due to the decreasing PAR selective layer thickness and changing in crosslinking extent that affects the microporosity of PAR. The phenomenon of N_2 permeance is mainly attributed to the crosslinking extent firstly increase and then decrease [47,48]. With increasing pH value from 10.65 to 11.60, the crosslinking extent of PAR selective layer increases due to the decrease of the addition of $NaHCO_3$, which leads to the decrease in ionic strength of the solution and the increase in solubility of TTSBI as the increasing pH value in aqueous solution. The increase of the monomer concentration in the aqueous solution is conducive to the degree of crosslinking [47,48], which was uneasy for N_2 molecule to transport through the porous channel of the membranes [46]. Moreover, the increasing degree of crosslinking that may lead to decrease in porosity contributes to the slow increase of CO_2 permeance, though the thickness of PAR selective layer obviously decreases. Afterwards, with the pH value varying from 12.20 to 12.85, the degree of hydrolysis of TMC severely increased, leading to a sharp decrease in the cross-linking extent, and even to defects. Thus, CO_2 and N_2 permeance sharply increase and CO_2/N_2 selectivity decreases. In addition, Fig. 6 clearly shows that the membrane prepared under pH = 11.60 has a CO_2 permeance of 870 GPU and a high CO_2/N_2 selectivity of 43, which confirms that the adjustment of pH value has successfully optimized the membrane structure and improved the membrane performance.

3.2. Effects of TTSBI concentration

In Section 3.1, the pH modifier $NaHCO_3$ decreases solubility of TTSBI in water under relatively low pH value and results in obvious changes in PAR structure and gas separation performance of membranes. Generally, the concentration of monomer in aqueous phase in IP also plays an important role in IP, which affects the reaction rate and the ratio of monomers in reaction zone in IP and results in changing of thickness and crosslinking density of formed membranes [47,48].

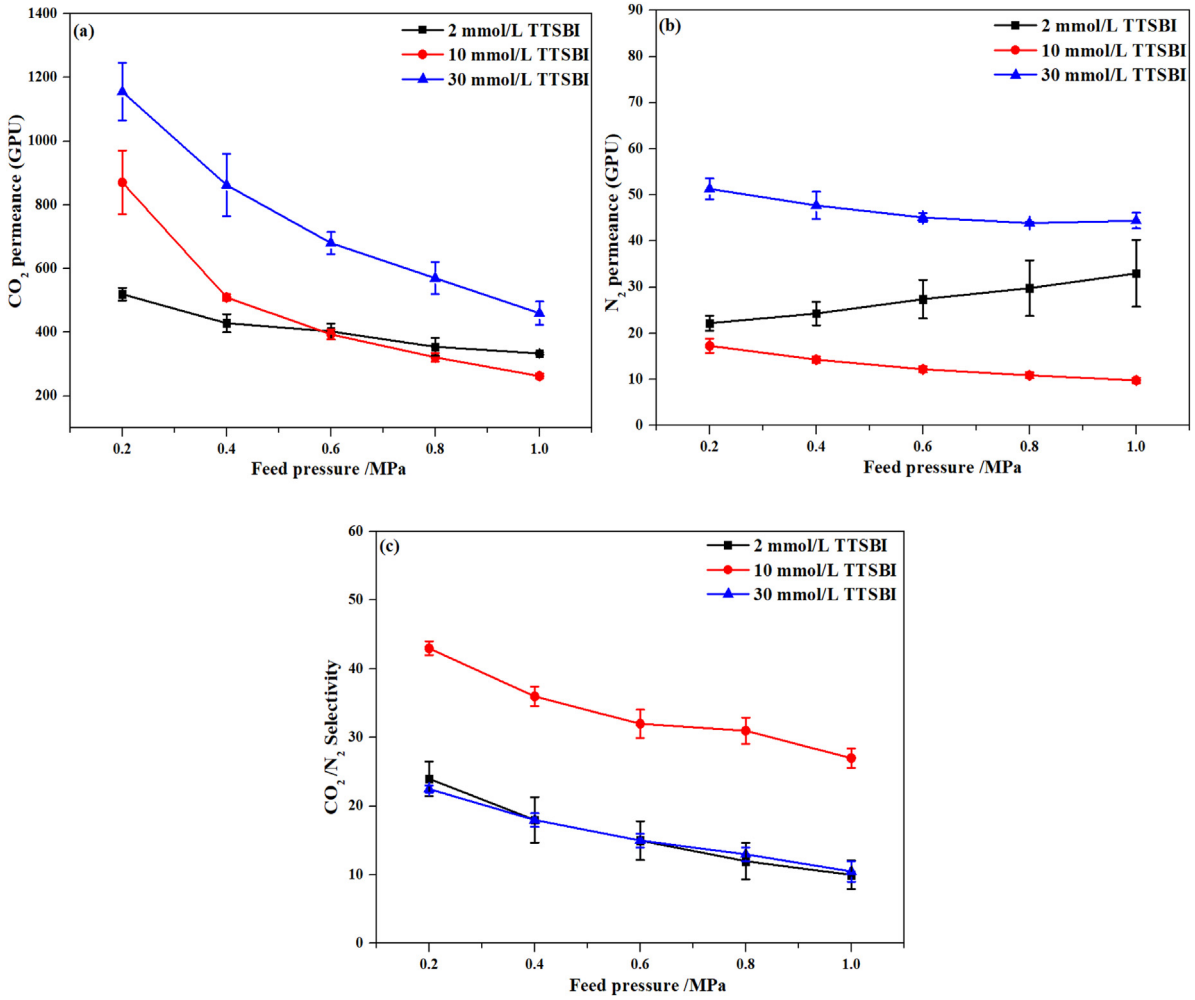

Fig. 9. (a) CO_2 permeance, (b) N_2 permeance and (c) CO_2/N_2 selectivity of microporous TFC membranes prepared with different TTSBI concentrations. All the pH value in aqueous phase is 11.60 and TMC concentration in hexane is 0.25 mmol/L. Water saturated CO_2/N_2 mixed gas (15% CO_2 and N_2 balance) was used as the feed gas.

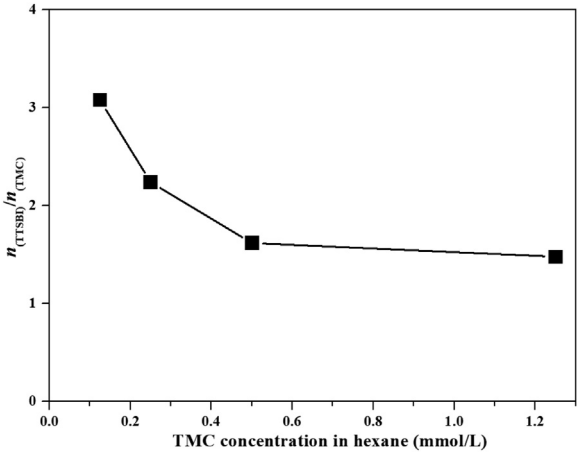

Fig. 10. The $n_{(TTSBI)}/n_{(TMC)}$ in PAR layer prepared with different TMC concentrations. All the pH value is 11.60 and TTSBI concentration is 10 mmol/L in aqueous phase.

Therefore, in this section, the effects of TTSBI concentration in aqueous solution were investigated under a constant pH value of 11.60 and 0.25 mmol/L TMC in hexane.

As shown in Fig. 7(a) and Table S4 in Supporting information, the content of -ONa increased only 8.06% with five-folds increasing in TTSBI concentration, i.e. from 2 mmol/L to 10 mmol/L. The variation of -ONa content is negligible compared with the changing in TTSBI concentration. Therefore, TTSBI concentration hardly affects the percentage of -ONa groups in TTSBI, which indicates that the hydrolysis of TTSBI is mainly affected by pH value of aqueous solution. Similar extent of hydrolysis of TMC could be expected at the same pH value of aqueous solution. However, the surface zeta potential of membranes in Fig. 7(b) shows that the membrane prepared with highest TTSBI concentration presents a relatively higher zeta potential. This is mainly due to more TTSBI-terminated polymer formed at high TTSBI concentration and increase in content of –OH group on the surface of membrane. The results are in accordance with the XPS analysis results shown in Fig. 7(c) (also see Fig. S5 and Table S5 in Supporting information), in which the ratio of TTSBI to TMC in PAR increases with increasing TTSBI concentration.

Cross-sectional SEM images of microporous TFC membranes prepared with different TTSBI concentrations are shown in Fig. 8. The PAR layer thickness in the microporous TFC membranes decreases from 110 nm to 45 nm with increasing TTSBI concentration. The reduced thickness is mainly caused by the self-inhibition reaction between TMC and TTSBI during the process of IP [61]. With increasing concentration of TTSBI, the reaction rate of TTSBI and TMC increases, resulting in an integrated network structure formed in a shorter time and decrease in the thickness of PAR [61].

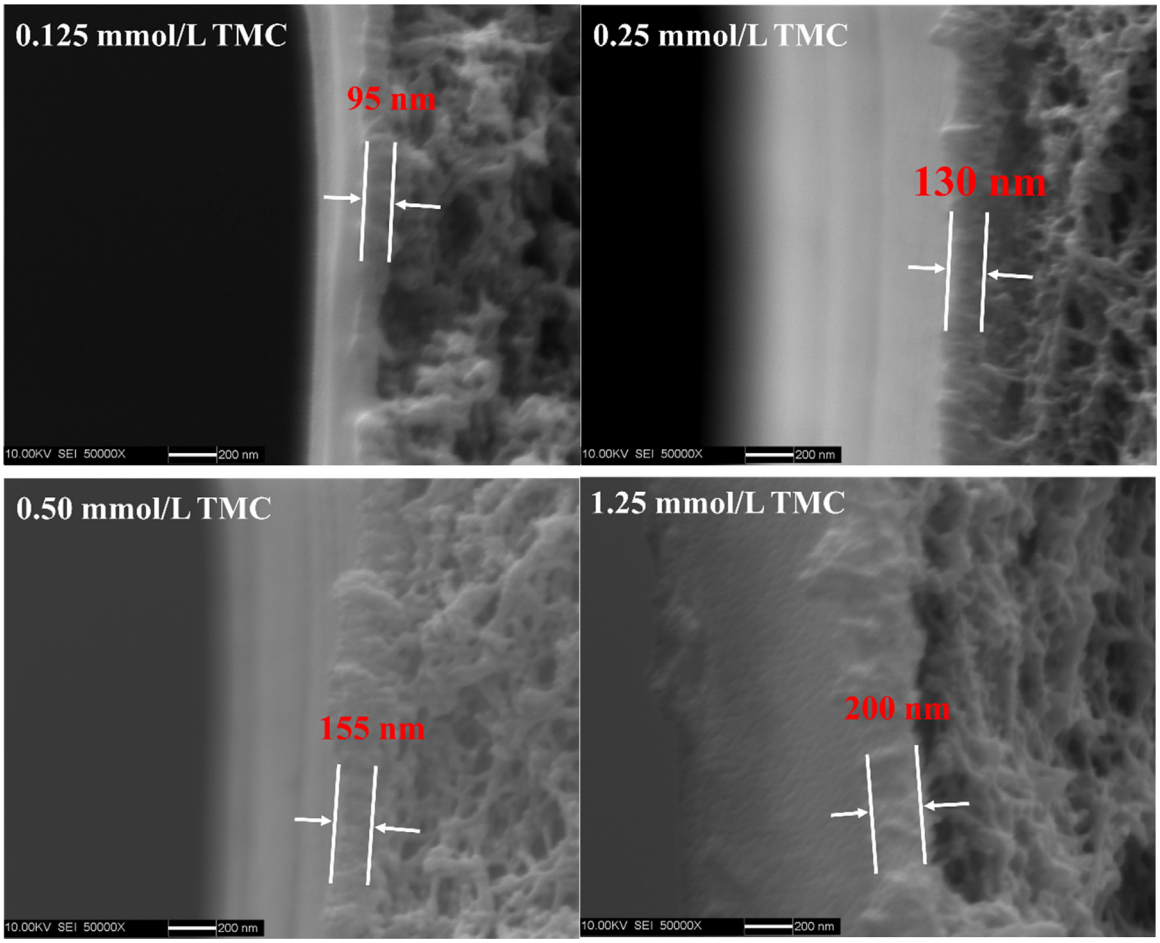

Fig. 11. Cross-sectional SEM images of microporous TFC membranes prepared with different TMC concentrations. All the pH value is 11.60 and TTSBI concentration is 10 mmol/L in aqueous phase.

Fig. 9 shows the influence of the TTSBI concentrations in the aqueous solution on CO_2/N_2 permeance and selectivity of microporous TFC membranes from 0.2 to 1.0 MPa. CO_2 permeance increases and N_2 permeance firstly decreases and then increases with increasing TTSBI concentration. When the TTSBI concentration is 2 mmol/L in aqueous solution, the relatively low CO_2 and N_2 permeance of the microporous TFC membrane attribute to the thick PAR selective layer. With increasing feed pressure, the N_2 permeance increases because of the swelling action of CO_2, which has been confirmed by single gas permeation test (see Fig. S6 in Supporting information) and indicates the PAR structure formed at low TTSBI concentration is loose and easy to be swelling by CO_2 [53]. Meanwhile, the loose structure contributes to the low CO_2/N_2 selectivity of the microporous TFC membrane. When the TTSBI concentration reaches 10 mmol/L in aqueous solution, the increasing CO_2 permeance and high CO_2/N_2 selectivity of the microporous TFC membrane were acquired. The appropriate TTSBI concentration facilitates the forming of highly crosslinked and compact PAR selective layer. With the TTSBI concentration up to 30 mmol/L in aqueous solution, both CO_2 and N_2 permeance were high due to the thinnest PAR layer as well as the inappropriate $n_{(TTSBI)}/n_{(TMC)}$ in PAR (see Table S5 in Supporting information), leading to the loosened PAR network. Thus, the CO_2 permeance reaches 1137 GPU but the CO_2/N_2 selectivity is only 22.

3.3. Effects of TMC concentration

In order to further manifest that the gas separation performance of the microporous TFC membranes prepared by IP is adjustable, the influence of TMC concentration on gas separation was investigated, in which the TTSBI concentration was 10 mmol/L and the pH value is 11.60 in aqueous solution. As shown in Fig. 10 (also see Fig. S7 and Table S6 in Supporting information), the XPS analysis results show the $n_{(TTSBI)}/n_{(TMC)}$ in PAR decreases with increasing TMC concentration, indicating the increasing content of TMC in PAR. The cross-sectional SEM images in Fig. 11 indicate that the PAR selective layer thickness increase rapidly from 15 nm to 120 nm with the increasing TMC concentrations, which is in accordance with literature reports [53].

CO_2/N_2 gas permeance and selectivity of the microporous TFC membranes prepared with different TMC concentrations are presented in Fig. 12. It can be found that both CO_2 and N_2 permeance are declined with the increasing TMC concentration on the whole which is mainly caused by the increasing thickness as shown in Fig. 11. The extremely high N_2 permeance and low CO_2/N_2 selectivity of the membrane prepared with 0.125 mmol/L TMC concentration is attributed to the low crosslinking extent [47]. The large error range is mainly caused by the defects formed under the lowest TMC concentration and the similar phenomenon has been also reported before [48,53].

3.4. Separation performance and stability comparison with other microporous polymer membranes

The comparison of gas separation performance of membranes in this work with other microporous polymer membranes and recent high-performance polymer membranes published in representative literature is presented in Fig. 13(a) (also in Table S7 in Supporting information). Compared with PAR membranes reported in the literature [46], the

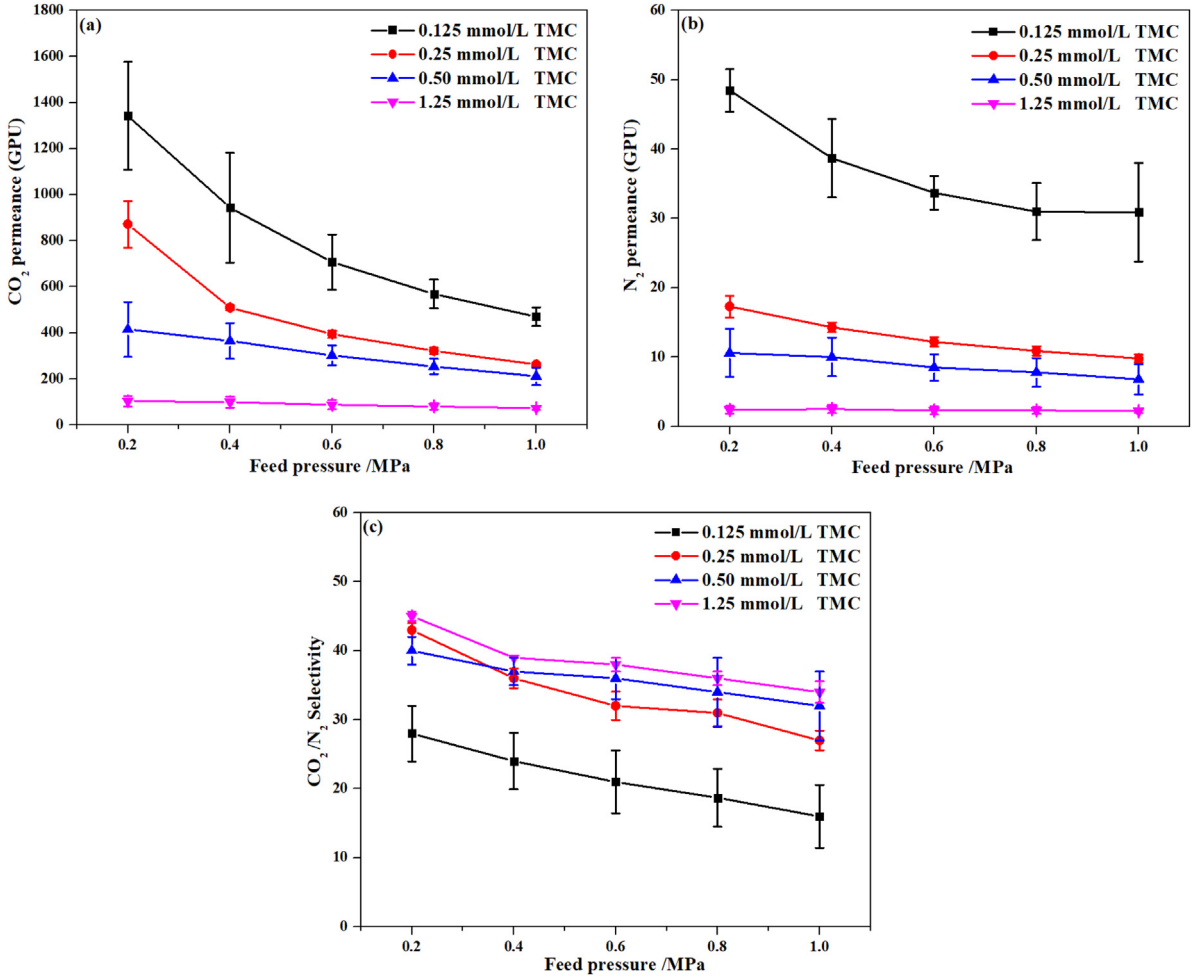

Fig. 12. (a) CO_2 permeance, (b) N_2 permeance and (c) CO_2/N_2 selectivity of microporous TFC membranes prepared with different TMC concentrations. All the pH value is 11.60 and TTSBI concentration is 10 mmol/L in aqueous phase. Water saturated CO_2/N_2 mixed gas (15% CO_2 and N_2 balance) was used as the feed gas.

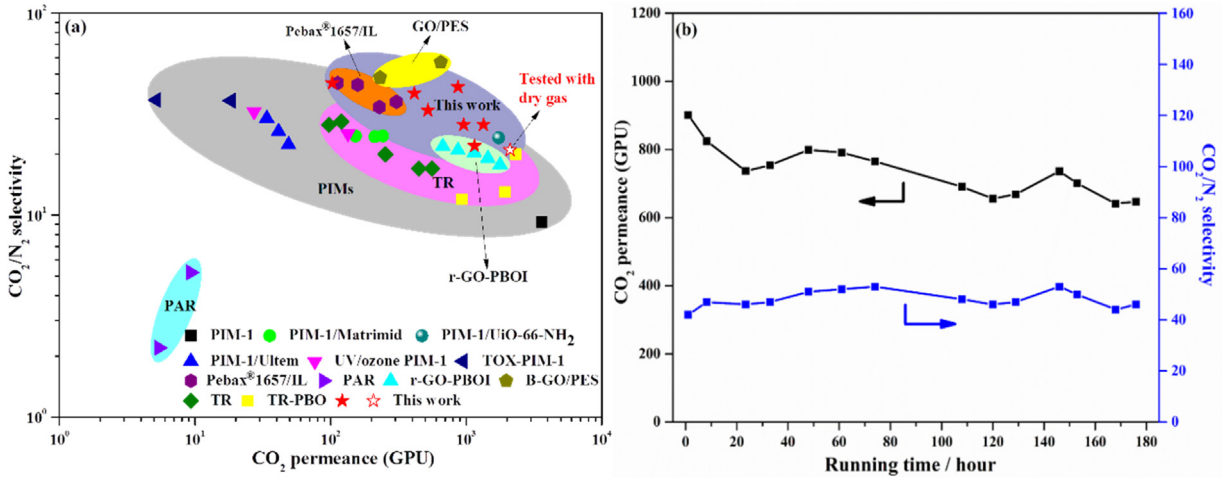

Fig. 13. (a) Performance comparison of membranes obtained in this work with other reported ultrathin microporous polymer membranes and recent high-performance polymer membranes [20,22–26,31,33,46,63,64,66–68]; (b) Variations of CO_2 permeance and CO_2/N_2 selectivity of the microporous TFC membrane for continuous separation with 0.25 mmol/L concentration of TMC solution, 10 mmol/L concentration of TTSBI solution and pH = 11.60. Feed gas pressure: 0.20 MPa. Feed flow: 1.5 L/min. Feed gas: CO_2/N_2 (15/85 vol%) mixed gases.

membranes in this work show hundreds times higher CO_2 permeance and ten times higher CO_2/N_2 selectivity. There are two main reasons for the better CO_2/N_2 separation performance of membranes in this work. The first one is the optimized structure of PAR for gas separation, especially the adequate crosslinking structures. The second one is the water-saturated feed gas applied in performance test. The water presenting in the actual flue gas stream could increase CO_2/N_2 selectivity of membranes due to the affinity of water to CO_2 [62]. In order to

confirm the effects of water in feed gas, the membrane in this work was also tested with dry gas. Compared with the results tested by humid gas, the CO_2 permeance increases from 870 GPU to 2115 GPU, and the CO_2/N_2 selectivity decreases from 43 to 21 which is still much higher than that reported in the literature [46]. As shown in Fig. 13(a), the membranes in this work show higher CO_2/N_2 selectivity than other reported ultrathin r-GO-PBOI membranes, TR polymer membranes, and PIM membranes. This is also attributed to the adequate crosslinking structures formed by IP and the water in feed gas. Compared with Pebax®1657/IL membranes and GO/PES membranes [63,64], the TFC membranes synthesized by IP technique show higher CO_2 permeance with comparable or slightly lower CO_2/N_2 selectivity [43,44]. In addition, it is worth noting that the membranes prepared in this work have CO_2 permeance in a wide range of 100–2115 GPU and the CO_2/N_2 selectivity of 45–21. The broad separation performance range is useful during the actual separation process, as the requirement for membrane performances in different separation stages are different in membrane process [32]. Therefore, the microporous TFC membranes based on IP are expected to meet different needs of industrial application.

As the physical aging of microporous polymer membranes is one of the main concerns that prevent the practical applications, the separation performance stability of the membrane was investigated through continuous gas permeation test conducted with humid CO_2/N_2 (15/85 vol%) mixed gas under 0.20 MPa at 22 °C. It's reported that the decrease in gas permeance or permeability of micro-porous polymer membranes was occurred in the first week and then it would be almost stable for about one year [33]. Thus, the gas separation performance of the membrane in this work was monitored for 180 h. As illustrated in Fig. 13(b), the CO_2 permeance of the membrane occurs the drop in the first 40 h and then fluctuated in a range of 600–800 GPU. During the period of the continuous gas permeation test, the CO_2 permeance decreased from 900 GPU to 640 GPU by 29%. However, during the 180 h operation, the CO_2/N_2 selectivity of the membrane kept a relatively high value over time. Although the membrane also suffers from the physical aging, but the decreasing rate of CO_2 permeance is much lower than both reported thick PIM membranes and thick crosslinking PIM (TOX-PIM-1) membranes which loss about 50% CO_2 permeability in a week [33,65]. The decrease of the CO_2 permeance in this work is comparable to the TR membrane with a thickness of 1.2 μm, which decreased about 26% after 200 h [37]. It's worth to mention that, the physical aging of ultrathin membrane is generally much more serious than thick membranes [38]. Thus, the microporous PAR membrane in this work show significant advances in performance stability than reported PIM membranes, which is expected to push the particle applications of microporous polymer membranes.

4. Conclusions

The ultrathin microporous polymer membranes possessing high gas separation performance have been prepared by IP. The effects pH values of aqueous phase, concentrations of TTSBI and TMC on structures of microporous PAR and separation performance were investigated. The pH value affects hydrolysis of both TTSBI and TMC, which results in decrease in $n_{(TTSBI)}/n_{(TMC)}$ in PAR with increasing pH value, implying changes in crosslinking structure. The thickness of PAR layer decreases with increasing pH value due to the increase in hydrolysis degree of TMC. Moreover, the concentrations of TTSBI and TMC also affects the crosslinking structure and PAR layer thickness. The $n_{(TTSBI)}/n_{(TMC)}$ in PAR has a significant effect on the microporous structure of PAR. Thus, the gas separation performance was manifested by adjusting IP parameters and optimizing the membrane structures. The resulted membranes exhibit CO_2 permeance in a wide range of 100–2115 GPU with the CO_2/N_2 selectivity of 45–21 that shows significant advantages over reported ultrathin microporous polymer membranes. In addition, only 29% decrease in CO_2 permeance was observed after 180 h aging, which is expected to push the particle applications of microporous polymer membranes.

Acknowledgement

This research is supported by the National Natural Science Foundation of China (No. 21606212), China Scholarship Council (CSC), the Priority Academic Program Development of Jiangsu Higher Education Institutions (PAPD), and Postgraduate Research & Practice Innovation Program of Jiangsu Province (KYCX17_0989).

Appendix A. Supplementary material

Supplementary data associated with this article can be found in the online version at doi:10.1016/j.memsci.2018.12.029

References

[1] D.S. Sholl, R.P. Lively, Seven chemical separations to change the world, Nature 532 (2016) 435–437.
[2] J.P. Jung, C.H. Park, J.H. Lee, Y.-S. Bae, J.H. Kim, Room-temperature, one-pot process for CO_2 capture membranes based on PEMA-g-PPG graft copolymer, Chem. Eng. J. 313 (2017) 1615–1622.
[3] W.J. Koros, C. Zhang, Materials for next-generation molecularly selective synthetic membranes, Nat. Mater. 16 (2017) 289–297.
[4] H.B. Park, J. Kamcev, L.M. Robeson, M. Elimelech, B.D. Freeman, Maximizing the right stuff: the trade-off between membrane permeability and selectivity, Science 356 (2017) 1138–1148.
[5] X. Zou, G. Zhu, Microporous organic materials for membrane-based gas separation, Adv. Mater. 30 (2018) 1700750.
[6] S. Kim, Y.M. Lee, Rigid and microporous polymers for gas separation membranes, Prog. Polym. Sci. 43 (2015) 1–32.
[7] G. Dong, Y.M. Lee, Microporous polymeric membranes inspired by adsorbent for gas separation, J. Mater. Chem. A 5 (2017) 13294–13319.
[8] G. Kupgan, L.J. Abbott, K.E. Hart, C.M. Colina, Modeling amorphous microporous polymers for CO_2 capture and separations, Chem. Rev. 118 (2018) 5488–5538.
[9] L.M. Robeson, M.E. Dose, B.D. Freeman, D.R. Paul, Analysis of the transport properties of thermally rearranged (TR) polymers and polymers of intrinsic microporosity (PIM) relative to upper bound performance, J. Membr. Sci. 525 (2017) 18–24.
[10] N.B. Mckeown, S. Hanif, K. Msayib, C.E. Tattershall, P.M. Budd, Porphyrin-based nanoporous network polymers, Chem. Commun. 23 (2002) 2782.
[11] P.M. Budd, B. Ghanem, K. Msayib, N.B. Mckeown, C. Tattershall, A nanoporous network polymer derived from hexaazatrinaphthylene with potential as an adsorbent and catalyst support, J. Mater. Chem. A. 13 (2003) 2721–2726.
[12] P.M. Budd, B.S. Ghanem, S. Makhseed, N.B. Mckeown, K.J. Msayib, C.E. Tattershall, Polymers of intrinsic microporosity (PIMs): robust, solution-processable, organic nanoporous materials, Chem. Commun. 2 (2004) 230.
[13] P.M. Budd, E.S. Elabas, B.S. Ghanem, S. Makhseed, N.B. McKeown, K.J. Msayib, C.E. Tattershall, D. Wang, Solution-processed, organophilic membrane derived from a polymer of intrinsic microporosity, Adv. Mater. 16 (2004) 456–459.
[14] P. Budd, K. Msayib, C. Tattershall, B. Ghanem, K. Reynolds, N. McKeown, D. Fritsch, Gas separation membranes from polymers of intrinsic microporosity, J. Membr. Sci. 251 (2005) 263–269.
[15] C.G. Bezzu, M. Carta, A. Tonkins, J.C. Jansen, P. Bernardo, F. Bazzarelli, N.B. McKeown, A spirobifluorene-based polymer of intrinsic microporosity with improved performance for gas separation, Adv. Mater. 24 (2012) 5930–5933.
[16] H.B. Park, C.H. Jung, Y.M. Lee, A.J. Hill, S.J. Pas, S.T. Mudie, E. Van Wagner, B.D. Freeman, D.J. Cookson, Polymers with cavities tuned for fast selective transport of small molecules and ions, Science 318 (2007) 254–258.
[17] K.A. Stevens, Z.P. Smith, K.L. Gleason, M. Galizia, D.R. Paul, B.D. Freeman, Influence of temperature on gas solubility in thermally rearranged (TR) polymers, J. Membr. Sci. 533 (2017) 75–83.
[18] Q. Liu, D.R. Paul, B.D. Freeman, Gas permeation and mechanical properties of thermally rearranged (TR) copolyimides, Polymer 82 (2016) 378–391.
[19] Y. Zhuang, J.G. Seong, W.H. Lee, Y.S. Do, M.J. Lee, G. Wang, M.D. Guiver, Y.M. Lee, Mechanically tough, thermally rearranged (TR) random/block poly(benzoxazole-co-imide) gas separation membranes, Macromolecules 48 (2015) 5286–5299.
[20] M. Wang, J. Zhao, X. Wang, A. Liu, K.K. Gleason, Recent progress on submicron gas-selective polymeric membranes, J. Mater. Chem. A 5 (2017) 8860–8886.
[21] R.W. Baker, Membranes and Modules, John Wiley & Sons, Ltd, 2012.
[22] R.W. Baker, B.T. Low, Gas separation membrane materials: a perspective, Macromolecules 47 (2014) 6999–7013.
[23] P. Gorgojo, S. Karan, H.C. Wong, M.F. Jimenez-Solomon, J.T. Cabral, A.G. Livingston, Ultrathin polymer films with intrinsic microporosity: anomalous solvent permeation and high flux membranes, Adv. Funct. Mater. 24 (2014) 4729–4737.
[24] W.F. Yong, F.Y. Li, Y.C. Xiao, T.S. Chung, Y.W. Tong, High performance PIM−1/Matrimid hollow fiber membranes for CO_2/CH_4, O_2/N_2 and CO_2/N_2 separation, J. Membr. Sci. 443 (2013) 156–169.
[25] B. Ghalei, K. Sakurai, Y. Kinoshita, K. Wakimoto, Ali P. Isfahani, Q. Song,

K. Doitomi, S. Furukawa, H. Hirao, H. Kusuda, S. Kitagawa, E. Sivaniah, Enhanced selectivity in mixed matrix membranes for CO_2 capture through efficient dispersion of amine-functionalized MOF nanoparticles, Nat. Energy 2 (2017) 17086.
[26] K.T. Woo, J. Lee, G. Dong, J.S. Kim, Y.S. Do, H.J. Jo, Y.M. Lee, Thermally rearranged poly(benzoxazole -co- imide) hollow fiber membranes for CO_2 capture, J. Membr. Sci. 498 (2016) 125–134.
[27] K.T. Woo, G. Dong, J. Lee, J.S. Kim, Y.S. Do, W.H. Lee, H.S. Lee, Y.M. Lee, Ternary mixed-gas separation for flue gas CO_2 capture using high performance thermally rearranged (TR) hollow fiber membranes, J. Membr. Sci. 510 (2016) 472–480.
[28] M.L. Jue, V. Breedveld, R.P. Lively, Defect-free PIM-1 hollow fiber membranes, J. Membr. Sci. 530 (2017) 33–41.
[29] K.T. Woo, J. Lee, G. Dong, J.S. Kim, Y.S. Do, W.-S. Hung, K.-R. Lee, G. Barbieri, E. Drioli, Y.M. Lee, Fabrication of thermally rearranged (TR) polybenzoxazole hollow fiber membranes with superior CO_2/N_2 separation performance, J. Membr. Sci. 490 (2015) 129–138.
[30] J.H. Lee, J. Lee, H.J. Jo, J.G. Seong, J.S. Kim, W.H. Lee, J. Moon, D. Lee, W.J. Oh, J.-g. Yeo, Y.M. Lee, Wet CO_2 /N_2 permeation through a crosslinked thermally rearranged poly(benzoxazole- co -imide) (XTR-PBOI) hollow fiber membrane module for CO_2 capture, J. Membr. Sci. 539 (2017) 412–420.
[31] S. Kim, S.H. Han, Y.M. Lee, Thermally rearranged (TR) polybenzoxazole hollow fiber membranes for CO_2 capture, J. Membr. Sci. 403–404 (2012) 169–178.
[32] T.C. Merkel, H. Lin, X. Wei, R. Baker, Power plant post-combustion carbon dioxide capture: an opportunity for membranes, J. Membr. Sci. 359 (2010) 126–139.
[33] Q. Song, S. Cao, R.H. Pritchard, B. Ghalei, S.A. Al-Muhtaseb, E.M. Terentjev, A.K. Cheetham, E. Sivaniah, Controlled thermal oxidative crosslinking of polymers of intrinsic microporosity towards tunable molecular sieve membranes, Nat. Commun. 5 (2014) 4813.
[34] F.Y. Li, Y. Xiao, T.-S. Chung, S. Kawi, High-performance thermally self-cross-linked polymer of intrinsic microporosity (PIM-1) membranes for energy development, Macromolecules 45 (2012) 1427–1437.
[35] F.Y. Li, Y. Xiao, Y.K. Ong, T.-S. Chung, UV-rearranged PIM-1 polymeric membranes for advanced hydrogen purification and production, Adv. Energy Mater. 2 (2012) 1456–1466.
[36] B. Comesaña-Gandara, L. Ansaloni, Y. Lee, A. Lozano, M. De Angelis, Sorption, diffusion, and permeability of humid gases and aging of thermally rearranged (TR) polymer membranes from a novel ortho-hydroxypolyimide, J. Membr. Sci. 542 (2017) 439–455.
[37] H. Wang, T.-S. Chung, D.R. Paul, Physical aging and plasticization of thick and thin films of the thermally rearranged ortho-functional polyimide 6FDA–HAB, J. Membr. Sci. 458 (2014) 27–35.
[38] C. Zhou, T.S. Chung, R. Wang, S. Hong Goh, A governing equation for physical aging of thick and thin fluoropolyimide films, J. Appl. Polym. Sci. 92 (2004) 1758–1764.
[39] L. Shao, J. Samseth, M.-B. Hägg, Crosslinking and stabilization of nanoparticle filled poly(1-trimethylsilyl-1-propyne) nanocomposite membranes for gas separations, J. Appl. Polym. Sci. 113 (2009) 3078–3088.
[40] G.A. Dibrov, V.V. Volkov, V.P. Vasilevsky, A.A. Shutova, S.D. Bazhenov, V.S. Khotimsky, A. van de Runstraat, E.L.V. Goetheer, A.V. Volkov, Robust high-permeance PTMSP composite membranes for CO_2 membrane gas desorption at elevated temperatures and pressures, J. Membr. Sci. 470 (2014) 439–450.
[41] M. Calle, H.J. Jo, C.M. Doherty, A.J. Hill, Y.M. Lee, Cross-linked thermally rearranged poly(benzoxazole-co-imide) membranes prepared from ortho-hydroxycopolyimides containing pendant carboxyl groups and gas separation properties, Macromolecules 48 (2015) 2603–2613.
[42] Y.S. Do, W.H. Lee, J.G. Seong, J.S. Kim, H.H. Wang, C.M. Doherty, A.J. Hill, Y.M. Lee, Thermally rearranged (TR) bismaleimide-based network polymers for gas separation membranes, Chem. Commun. 52 (2016) 13556–13559.
[43] G.D. Kang, Y.M. Cao, Development of antifouling reverse osmosis membranes for water treatment: a review, Water Res. 46 (2012) 584–600.
[44] L. Shao, X.Q. Cheng, Y. Liu, S. Quan, J. Ma, S.Z. Zhao, K.Y. Wang, Newly developed nanofiltration (NF) composite membranes by interfacial polymerization for Safranin O and Aniline blue removal, J. Membr. Sci. 430 (2013) 96–105.
[45] H. Qian, J. Zheng, S. Zhang, Preparation of microporous polyamide networks for carbon dioxide capture and nanofiltration, Polymer 54 (2013) 557–564.
[46] M.F. Jimenez-Solomon, Q. Song, K.E. Jelfs, M. Munoz-Ibanez, A.G. Livingston, Polymer nanofilms with enhanced microporosity by interfacial polymerization, Nat. Mater. 15 (2016) 760–767.
[47] F. Yuan, Z. Wang, S. Li, J. Wang, S. Wang, Formation–structure–performance correlation of thin film composite membranes prepared by interfacial polymerization for gas separation, J. Membr. Sci. 421–422 (2012) 327–341.
[48] M. Wang, Z. Wang, S. Li, C. Zhang, J. Wang, S. Wang, A high performance anti-oxidative and acid resistant membrane prepared by interfacial polymerization for CO_2 separation from flue gas, Energy Environ. Sci. 6 (2013) 539–551.
[49] S. Li, H. Zhang, S. Yu, J. Hou, S. Huang, Y. Liu, Pore structure characterization and gas transport property of the penetrating layer in composite membranes, Sep. Purif. Technol. 211 (2019) 252–258.
[50] S. Yu, S. Li, S. Huang, Z. Zeng, S. Cui, Y. Liu, Covalently bonded zeolitic imidazolate frameworks and polymers with enhanced compatibility in thin film nanocomposite membranes for gas separation, J. Membr. Sci. 540 (2017) 155–164.
[51] P.J. Milner, R.L. Siegelman, A.C. Forse, M.I. Gonzalez, T. Runčevski, J.D. Martell, J.A. Reimer, J.R. Long, A diaminopropane-appended metal–organic framework enabling efficient CO_2 capture from coal flue gas via a mixed adsorption mechanism, J. Am. Chem. Soc. 139 (2017) 13541–13553.
[52] B. Huang, S. Xu, S. Gao, L. Liu, J. Tao, H. Niu, M. Cai, J. Cheng, Industrial test and techno-economic analysis of CO_2 capture in Huaneng Beijing coal-fired power station, Appl. Energ. 87 (2010) 3347–3354.
[53] S. Li, Z. Wang, C. Zhang, M. Wang, F. Yuan, J. Wang, S. Wang, Interfacially polymerized thin film composite membranes containing ethylene oxide groups for CO_2 separation, J. Membr. Sci. 436 (2013) 121–131.
[54] R. Zhang, S. Yu, W. Shi, W. Wang, X. Wang, Z. Zhang, L. Li, B. Zhang, X. Bao, A novel polyesteramide thin film composite nanofiltration membrane prepared by interfacial polymerization of serinol and trimesoyl chloride (TMC) catalyzed by 4-dimethylaminopyridine (DMAP), J. Membr. Sci. 542 (2017) 68–80.
[55] T. Puspasari, N. Pradeep, K.-V. Peinemann, Crosslinked cellulose thin film composite nanofiltration membranes with zero salt rejection, J. Membr. Sci. 491 (2015) 132–137.
[56] W. Fang, L. Shi, R. Wang, Mixed polyamide-based composite nanofiltration hollow fiber membranes with improved low-pressure water softening capability, J. Membr. Sci. 468 (2014) 52–61.
[57] L. Li, S. Zhang, X. Zhang, Preparation and characterization of poly(piperazineamide) composite nanofiltration membrane by interfacial polymerization of 3,3′,5,5′-biphenyl tetraacyl chloride and piperazine, J. Membr. Sci. 335 (2009) 133–139.
[58] A. Manakhov, P. Kiryukhantsev-Korneev, M. Michlíček, E. Permyakova, E. Dvořáková, J. Polčák, Z. Popov, M. Visotin, D.V. Shtansky, Grafting of carboxyl groups using CO_2/C_2H_4/Ar pulsed plasma: theoretical modeling and XPS derivatization, Appl. Surf. Sci. 435 (2018) 1220–1227.
[59] M.R. Wertheimer, A.C. Fozza, A. Holländer, Industrial processing of polymers by low-pressure plasmas: the role of VUV radiation, Nucl. Instrum. Methods B 151 (1999) 65–75.
[60] L. Li, X. Yao, H. Li, Z. Liu, W. Ma, X. Liang, Thermal Stability of oxygen-containing functional groups on activated carbon surfaces in a thermal oxidative environment, J. Chem. Eng. Jpn. 47 (2014) 21–27.
[61] Y. Liu, B. He, J. Li, R.D. Sanderson, L. Li, S. Zhang, Formation and structural evolution of biphenyl polyamide thin film on hollow fiber membrane during interfacial polymerization, J. Membr. Sci. 373 (2011) 98–106.
[62] A. Hussain, M.-B. Hägg, A feasibility study of CO_2 capture from flue gas by a facilitated transport membrane, J. Membr. Sci. 359 (2010) 140–148.
[63] W. Fam, J. Mansouri, H. Li, V. Chen, Improving CO_2 separation performance of thin film composite hollow fiber with Pebax®1657/ionic liquid gel membranes, J. Membr. Sci. 537 (2017) 54–68.
[64] S. Wang, Y. Wu, N. Zhang, G. He, Q. Xin, X. Wu, H. Wu, X. Cao, M.D. Guiver, Z. Jiang, A highly permeable graphene oxide membrane with fast and selective transport nanochannels for efficient carbon capture, Energy Environ. Sci. 9 (2016) 3107–3112.
[65] R.R. Tiwari, J. Jin, B.D. Freeman, D.R. Paul, Physical aging, CO_2 sorption and plasticization in thin films of polymer with intrinsic microporosity (PIM-1), J. Membr. Sci. 537 (2017) 362–371.
[66] L. Hao, J. Zuo, T.S. Chung, Formation of defect-free polyetherimide/PIM-1 hollow fiber membranes for gas separation, AIChE J. 60 (2014) 3848–3858.
[67] Q. Song, S. Cao, P. Zavala-Rivera, L.P. Lu, W. Li, Y. Ji, S.A. Al-Muhtaseb, A.K. Cheetham, E. Sivaniah, Photo-oxidative enhancement of polymeric molecular sieve membranes, Nat. Commun. 4 (2013) 1918.
[68] S. Kim, J. Hou, Y. Wang, R. Ou, G.P. Simon, J.G. Seong, Y.M. Lee, H. Wang, Highly permeable thermally rearranged polymer composite membranes with a graphene oxide scaffold for gas separation, J. Mater. Chem. A 6 (2018) 7668–7674.